Scanning Tunneling Microscopy, Fourier Transform Infrared Spectroscopy, and Electrochemical Characterization of 2-Naphthalenethiol Self-Assembled Monolayers on the Au Surface: A Study of Bridge-Mediated Electron Transfer in $Ru(NH_3)_6^{2+}|Ru(NH_3)_6^{3+}$ Redox Reactions

V. Ganesh and V. Lakshminarayanan*

Raman Research Institute, C. V. Raman Avenue, Sadashivanagar, Bangalore 560080, India

Received: May 12, 2005; In Final Form: July 4, 2005

We have studied the structure, adsorption kinetics, and barrier properties of self-assembled monolayers of 2-naphthalenethiol on Au using electrochemical techniques, grazing-angle Fourier transform infrared (FTIR) spectroscopy, and scanning tunneling microscopy (STM). The results of cyclic voltammetric and impedance measurements using redox probes show that 2-naphthalenethiol on Au forms a stable and reproducible, but moderately blocking, monolayer. Annealing of the self-assembled monolayer (SAM)-modified surface at 72 ± 2 °C remarkably improves the blocking property of the monolayer of 2-naphthalenethiol on Au. From the study of kinetics of SAM formation, we find that the self-assembly follows Langmuir adsorption isotherm. Our STM and FTIR results show that the molecules are adsorbed with the naphthalene ring tilted from the surface normal by forming a $\sqrt{3} \times 3$ R30° overlayer structure. From our studies, we conclude that the electron-transfer reaction of ferro/ferricyanide in the freshly formed monolayer occurs predominantly through the pinholes and defects present in the monolayer. However, in the case of thermally annealed specimen, although the ferro/ferricyanide reaction is almost completely blocked, the electron-transfer reaction of hexaammineruthenium(III) chloride is not significantly inhibited. It is proposed that the electron-transfer reaction in the case of the ruthenium redox couple takes place by a tunneling mechanism through the high-electron-density aromatic naphthalene ring acting as a bridge between the monolayer-modified electrode and the ruthenium complex.

1. Introduction

Self-assembled monolayer (SAM) refers to a single layer of molecules on a substrate, which are adsorbed spontaneously by chemisorption and exhibit a high degree of orientation, molecular ordering, and packing density.[1] They have received a great deal of attention in recent times because of their potential application in a variety of fields, such as sensors,[2] photolithography,[3] nonlinear optical materials,[4] high-density memory storage devices,[5] and corrosion protection.[6] Even though adsorption of several functional groups on various metallic and nonmetallic surfaces has been reported in the literature, the thiols and disulfides on gold are the ones that have been extensively studied in recent times.[7] The various aspects of monolayer formation, structure, packing, orientation, wetting properties, and stability have been examined using different techniques, such as Fourier transform infrared spectroscopy (FTIR), contact angle measurements, X-ray photoelectron spectroscopy (XPS), ellipsometry, and scanning probe microscopy (SPM). Although a complete characterization of SAMs depends on the above-mentioned techniques, the electrochemical techniques, namely, cyclic voltammetry (CV) and electrochemical impedance spectroscopy (EIS), can be used effectively to understand the packing density, surface coverage, and distribution of pinholes and defects in the formation of the monolayer.[7]

We find from the literature that there are much fewer reports on aromatic thiol monolayers in comparison with those of long chain aliphatic thiols. Aromatic thiol monolayers represent interesting systems because of the highly delocalized electron density and structural rigidity of the phenyl ring. There have been some studies on thiophenol and functionalized thiophenol SAMs on gold.[8] Vijayamohanan et al.[9] characterized the monolayer formation of naphthalene disulfide and naphtho[1,8-*cd*]-1,2-dithiol on Au and Ag using electrochemical techniques, STM, XPS, and surface-enhanced Raman spectroscopy (SERS). Apart from naphthalene disulfide, 1,4-dimethoxynaphthalene norbornylogous compounds were also reported and it was found that their electron-transfer rate is enhanced compared with that of their alkane analogues because of rigidity of the norbornylogous bridges.[10] Chang et al. reported (6-alkoxynaphth-2-yl)methanethiol SAMs on Au and Ag by characterizing them using contact angle measurements, ellipsometry, and reflection absorption IR spectroscopy and found that the naphthalene ring forms a herringbone structure with a tilted configuration.[11] Whitesides et al. investigated the metal−insulator−metal junction based on the SAM of 2-naphthalenethiol on Au and Ag by measuring the breakdown voltage and found that the SAM on the Au junction is mechanically stable but immediately breaks down on application of potential.[12] To the best of our knowledge, there is no report in the literature on the monolayer formation and characterization of naphthalenethiol on gold, except by Randall and Joseph.[13] These authors reported the formation of SAMs of 2-naphthalenethiol and bis(2-naphthyl) disulfide onto bulk gold using liquid chromatography and diode array spectroscopy and showed that the naphthalene ring is tilted to the Au surface normal. There is, however, no report on the

* Corresponding author. E-mail address: narayan@rri.res.in. Phone: +91-80-23610122. Fax: +91-80-23610492..

10.1021/jp052489u CCC: $30.25
Published on Web 08/09/2005

electrochemical characterization, determination of surface coverage based on pinhole defect analysis, study on kinetics of SAM formation, or structural arrangement of SAMs of 2-naphthalenethiol on Au.

In this paper, we report the results of our study on the self-assembled monolayer of 2-naphthalenethiol on Au and its characterization using electrochemical, FTIR, and STM techniques. We have used electrochemical techniques such as cyclic voltammetry (CV) and electrochemical impedance spectroscopy (EIS) for the study of the barrier properties of the monolayer, such as its ordering and packing. We have also studied the electron-transfer process of two important redox systems, viz., $[Fe(CN)_6]^{3-|4-}$ and $[Ru(NH_3)_6]^{2+|3+}$, on the 2-naphthalenethiol monolayer-modified electrode. In addition, EIS measurements are used for the determination of the surface coverage and pinholes and defects analysis. The kinetics of adsorption of the monolayer on Au is also investigated using impedance measurements. Grazing-angle FTIR spectroscopy, STM, and interfacial capacitance studies are used to determine the orientation and structural arrangement of SAMs on Au. The effects of potential-cycling and annealing processes on the barrier property and structural arrangement of monolayers have also been investigated.

2. Experimental Section

2.1. Chemicals. All of the chemical reagents used in this study were AR grade reagents. 2-Naphthalenethiol (Aldrich), ethanol (99.95%; Merck), lithium perchlorate (Acros Organics), potassium ferrocyanide (Loba), potassium ferricyanide (Qualigens), sodium fluoride (Qualigens), perchloric acid (Qualigens), and hexaammineruthenium(III) chloride (Alfa Aesar) were used in our study. Millipore water having a resistivity of 18 MΩ cm was used to prepare the aqueous solutions.

2.2. Electrodes and Cells. Evaporated gold (∼100 nm thickness) on glass with chromium underlayers (2−5 nm thickness) was used as the substrate for SAM formation and characterization. The substrate was heated to 350 °C during gold evaporation under a vacuum pressure of 2×10^{-5} mbar, a process that normally yields a substrate with predominantly Au(111) orientation. The evaporated gold samples were used as strips for electrochemical studies. We have also carried out the electrochemical experiments with a gold wire as a working electrode, which was constructed by proper sealing of a 99.99% pure gold wire (Arora Mathey) of 0.5 mm diameter with soda lime glass having a thermal expansion coefficient close to that of gold. The electrode has a geometric area of 0.002 cm^2. This small-area working electrode has a highly reproducible true surface area (as measured by potential cycling in 0.1 M perchloric acid), even after repeated usage. A conventional three-electrode electrochemical cell was used for this study. A platinum foil of large surface area was used as the counter electrode, and a saturated calomel electrode (SCE) was used as the reference electrode. The cell was cleaned thoroughly before each experiment and kept in a hot-air oven at 100 °C for at least 1 h before the start of the experiment.

2.3. Electrode Pretreatment and Thiol Adsorption. Immediately before use, the gold wire electrode was polished with emery paper of grade 800 and 1500, followed by polishing in aqueous slurries of progressively finer alumina (1.0, 0.3, and 0.05 μm sizes), and ultrasonicated to remove alumina particles. Then, it was cleaned in a "piranha" solution (a mixture of 30% H_2O_2 and concentrated H_2SO_4 in a 1:3 ratio). *(Caution! Piranha solution is very reactive with organic compounds and storing in a closed container and exposure to direct contact should be avoided.)* Finally, it was rinsed in distilled water thoroughly, followed by rinsing in Millipore water before SAM formation. In the case of evaporated Au, the strips were used for SAM formation and it was pretreated with piranha solution. The monolayers were prepared by keeping the gold electrode in 20 mM 2-naphthalenethiol in ethanol for 1 h. After the adsorption of thiol, the electrode was rinsed with ethanol, distilled water, and finally with Millipore water. For the grazing-angle FTIR spectroscopy and STM analysis, evaporated Au samples were used as strips for thiol adsorption.

2.4. Electrochemical Characterization. Cyclic voltammetry and electrochemical impedance spectroscopy were used for electrochemical characterization of SAM-modified electrodes. The barrier property of the monolayer has been evaluated by studying the electron-transfer reaction using two different redox probes, namely, potassium ferrocyanide (negative redox probe) and hexaammineruthenium(III) chloride (positive redox probe). Cyclic voltammetry was performed in two different solutions, viz., 10 mM potassium ferrocyanide in 1 M sodium fluoride at a potential range of −0.1 to +0.5 V vs SCE and 1 mM hexaammineruthenium(III) chloride in 0.1 M lithium perchlorate at a potential range of −0.4 to +0.1V vs SCE. The impedance measurements were carried out using an alternating current (ac) of a 10-mV amplitude signal at a formal potential of the redox couple in solution containing always equal concentrations of both the oxidized and reduced forms of the redox couple, namely, 10 mM potassium ferrocyanide and 10 mM potassium ferricyanide in 1 M NaF. A wide frequency range of 100 kHz to 0.1 Hz was used for impedance measurements. The Au oxide stripping analysis was conducted in 0.1 M perchloric acid in the potential range 0.2−1.4 V vs SCE. Adsorption kinetics studies were carried out in 10 μM 2-naphthalenethiol and 0.1 M $LiClO_4$ in ethanol solution at different potentials, using evaporated Au electrodes as strips, by measuring the real and imaginary components of impedance. All the experiments were performed at room temperature.

2.5. Instrumentation. Cyclic voltammetry was carried out using an EG&G potentiostat (model 263A) interfaced to a PC through a GPIB card (National Instruments). The potential ranges and scan rates used are shown in the respective diagrams. For electrochemical impedance studies, the potentiostat was used along with an EG&G 5210 lock-in amplifier controlled by Power Sine software. For adsorption kinetics studies of monolayer formation, an EG&G potentiostat (model 263A) along with an EG&G 5210 lock-in amplifier interfaced to a PC was used. The real and imaginary components of impedance were acquired at a sampling rate of 100 ms for the initial 20 s and at 1 s for the remaining time. The data acquisition was carried out using a PCL 203A (Dyanalog) data acquisition card interfaced with LabTech notebook software.

A home-built scanning tunneling microscope (STM) in high-resolution mode described elsewhere[14] was used to probe the SAM-modified gold surface. STM images were obtained at room temperature in air, and the instrument was operated in constant current mode of 1 nA at a sample bias voltage of +100 mV. Prior to these experiments, the instrument was calibrated with highly oriented pyrolytic graphite (HOPG) (ZYA grade; Advanced Ceramic). An electrochemically etched tungsten tip was used as the probe. The images shown here were plane-corrected and Fourier-filtered using scanning probe image processor (SPIP) software (Image Metrology, Denmark). To ensure that the images shown were representative of the monolayer morphology, multiple images were taken at different locations and scan ranges.

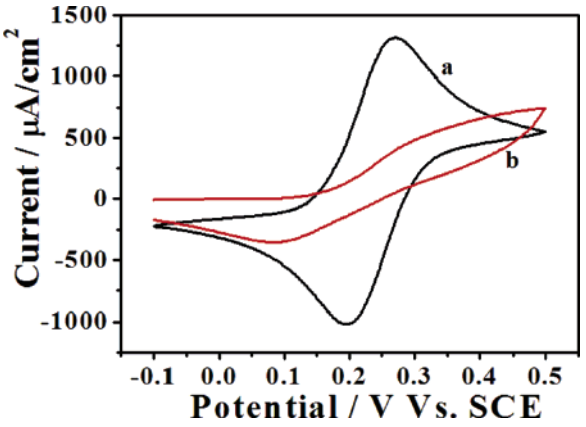

Figure 1. Cyclic voltammograms of (a) a bare Au electrode and (b) the SAM of a 2-naphthalenethiol-modified Au electrode in 10 mM potassium ferrocyanide with 1 M NaF as supporting electrolyte at a potential scan rate of 50 mV/s.

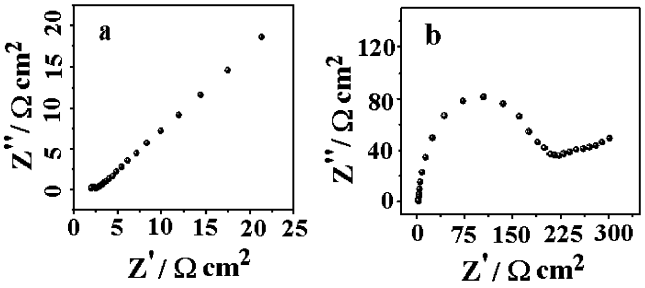

Figure 2. Impedance plots in 10 mM potassium ferrocyanide and 10 mM potassium ferricyanide with 1 M NaF as supporting electrolyte for (a) a bare Au electrode and (b) a monolayer of a 2-naphthalenethiol-coated Au electrode.

The FTIR spectra were obtained using a FTIR 8400 model (SHIMADZU) with a fixed 85° grazing-angle attachment (FT-85; Thermo Spectra-Tech).

3. Results and Discussion

3.1. Electrochemical Characterization. Cyclic voltammetry and electrochemical impedance spectroscopy have been used for the electrochemical characterization of the monolayer. Figure 1 shows the cyclic voltammogram of a bare gold electrode (Figure 1a) and a 2-naphthalenethiol-modified gold electrode (Figure 1b) in 10 mM potassium ferrocyanide with 1 M NaF as the supporting electrolyte at a potential scan rate of 50 mV/s. It can be seen that the bare gold electrode shows a reversible peak for the redox couple, indicating that the reaction is diffusion-controlled. In contrast, for the SAM-modified electrode, the CV exhibits an irreversible behavior with a large peak separation and significant peak currents, indicating that the electron-transfer reaction occurs by an irreversible process. Such a behavior is typical of a monolayer with rather poor blocking properties to the redox species.

Figure 2 shows the impedance plots of the bare gold electrode and the SAM-modified electrode in equal concentrations of potassium ferro/ferricyanide with 1 M NaF as the supporting electrolyte. Figure 2a shows a straight line at a low frequency and a very small semicircle at a high-frequency region, indicating that the process is essentially diffusion-controlled for the redox couple on a bare gold electrode. The impedance plot of the SAM-modified electrode in Figure 2b shows the behavior of a blocking monolayer with a well-defined semicircle at higher frequencies. The equivalent circuit is fitted to a Randle's model with parallel charge-transfer resistance, R_{ct}, and CPE (constant phase element) with a series uncompensated solution resistance, R_u. From the fitting, a R_{ct} of 0.55 Ω cm² is measured for the bare gold electrode and the monolayer-modified electrode shows a higher R_{ct} value of 190 Ω cm². This value is lower compared with the R_{ct} value of about 284 Ω cm² for comparable concentration reported for the SAM of naphthalene disulfide on Au by Vijayamohanan et al.[9f]

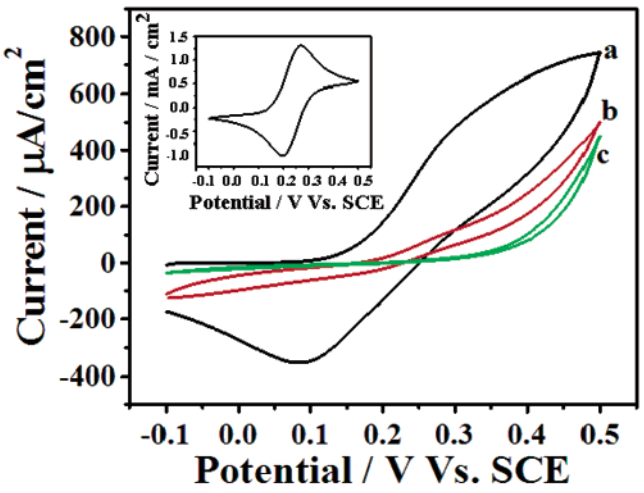

Figure 3. Cyclic voltammograms in 10 mM potassium ferrocyanide with 1 M NaF as supporting electrolyte at a potential scan rate of 50 mV/s for (a) the SAM of a 2-naphthalenethiol-modified Au electrode, (b) a potential-cycled electrode after the SAM formation of 2-naphthalenethiol on Au, and (c) an annealed electrode after the SAM formation of 2-naphthalenethiol on Au. Inset shows the cyclic voltammogram of a bare Au electrode in the same solution for comparison.

We have tried to improve the blocking behavior of the monolayer-modified electrode by two different processes, namely by subjecting the freshly formed SAM to (i) potential cycling in a pure supporting electrolyte and (ii) annealing at 72 ± 2 °C.

3.2. Effect of Potential Cycling and Annealing. Immediately after the monolayer formation, the electrode is potential-cycled between 0.0 and 0.6 V vs SCE in 1 M NaF without any redox species and the same electrode is used for the cyclic voltammetry and impedance spectroscopy studies to determine the barrier property. In the case of annealing, after the thiol adsorption, the gold electrode is taken out, washed completely, and immediately kept in a hot-air oven for ca. $^1/_2$ h at 72 ± 2 °C. It is then allowed to cool to room temperature and used for the studies.

Figure 3 shows the CVs of the monolayer-modified, potential-cycled, and annealed (after the SAM formation) electrodes in 10 mM potassium ferrocyanide with 1 M NaF as the supporting electrolyte and at a potential scan rate of 50 mV/s. For comparison, the cyclic voltammogram of a bare gold electrode for the same redox reaction is also shown in the inset of Figure 3.

Figure 3a shows an irreversible peak formation for the SAM-modified electrode. In contrast, the potential-cycled electrode shows a better blocking behavior for the redox reaction (Figure 3b). However, the barrier property of the SAM-modified electrode dramatically improves after annealing, as seen from Figure 3c. It is evident from the CVs that the electron-transfer reaction through the monolayer film is almost totally inhibited, a process that can only be attributed to more compact organization and structural modification of the monolayer after annealing.

Figure 4a,b shows, respectively, the impedance plots of potential-cycled and annealed electrodes (after SAM formation) in equal concentrations of potassium ferro/ferricyanide with NaF

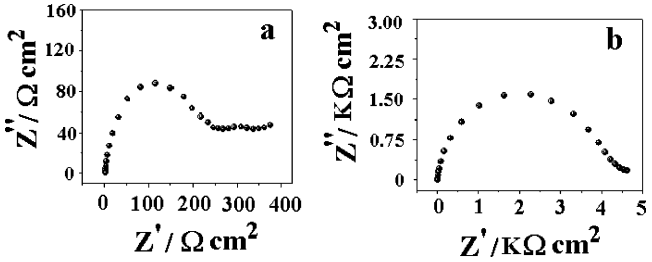

Figure 4. Impedance plots in a solution of 10 mM potassium ferrocyanide and 10 mM potassium ferricyanide with 1 M NaF as supporting electrolyte for (a) a potential-cycled electrode after the monolayer formation and (b) an annealed electrode after the monolayer formation.

TABLE 1: R_{ct} Values Obtained from the Equivalent Circuit-Fitting Analysis of Impedance Data for Various Electrodes

sample	R_{ct} (Ω cm^2) $Fe(CN)_6^{3-}$ | $Fe(CN)_6^{4-}$	R_{ct} (Ω cm^2) $Ru(NH_3)_6^{2+}$ | $Ru(NH_3)_6^{3+}$
bare Au	0.55	1.26
SAM of 2-NT on Au	190	5.00
potential-cycled SAM	221	11.59
annealed SAM	3854	34.75

as the supporting electrolyte. The impedance values are fitted to standard Randle's equivalent circuit, comprising of faradaic impedance Z_f, which is parallel to a constant phase element (CPE) represented by Q, and in a series with the uncompensated solution resistance R_u. The faradaic impedance, Z_f, is a series combination of charge-transfer resistance, R_{ct}, and the Warburg impedance, W.

Table 1 shows the values obtained from the fitting of impedance values for various samples. It can be seen from the table that the R_{ct} values, as expected, are higher for the monolayer-modified electrodes than for the bare gold electrodes. The SAM-modified electrode, after potential cycling in 1 M NaF, shows very little increase in the R_{ct} value when compared to that of the fresh monolayer-coated electrode, which implies that the charge-transfer process is inhibited only marginally by the potential-cycling process. This is in contrast to the CV behavior, as seen in Figure 3b, for the electode, which is potential-cycled and has a shape that suggests a more blocking behavior than the freshly formed SAM. This behavior implies a possibility of some structural reorganization of the monolayer due to potential cycling without significantly affecting the ionic permeability to the redox species, as revealed by the R_{ct} values. Such behavior was also reported earlier in the case of aliphatic thiol monolayers.[15−18] The fact that the R_{ct} value is very high (3854 Ω cm^2) for the annealed SAM suggests that the barrier property of the monolayer to the electron-transfer reaction has improved remarkably, and it is almost completely under charge-transfer control. The impedance diagram of the redox reaction on the annealed SAM (Figure 4b) shows a large semicircle in the entire range of frequencies. This is fitted to a parallel combination of Q (CPE) and charge-transfer resistance, R_{ct}, with a series uncompensated solution resistance of R_u. The R_{ct} value of 3854 Ω cm^2, reported here for the SAM of 2-naphthalenethiol on Au, is much higher when compared with the literature values[9b,d,f] of about 284, 550, and 650 Ω cm^2 for the respective SAMs of naphthalene disulfide (NDS), diphenyl diselenide (DDSe), and diphenyl disulfide (DDS) on gold for comparable concentrations which implies the compact and highly dense formation of SAM of 2-naphthalenethiol on Au.

From the impedance diagram (Figure 4), it can be seen that there is a low-frequency component in the case of the SAM-modified electrodes (including the potential-cycled and annealed samples), which can arise because of slow ionic diffusion through the pinholes and defects present in the SAM. This low-frequency diffusion region is significantly smaller in the case of the annealed sample. For the equivalent circuit-fitting analysis of impedance values, we have considered only the semicircle component and fitted the data from 100 kHz to 1 Hz. The measured R_{ct} values are shown in Table 1.

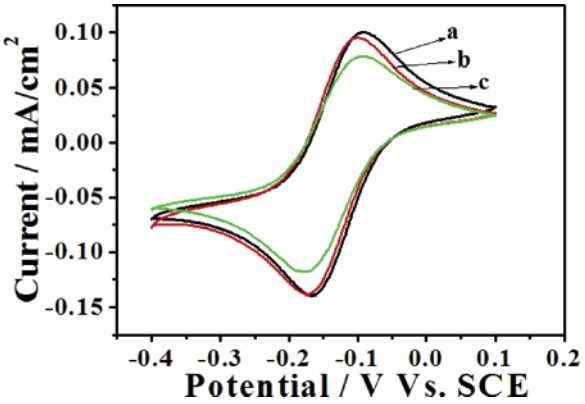

Figure 5. Cyclic voltammograms in 1 mM hexaammineruthenium-(III) chloride with 0.1 M $LiClO_4$ as supporting electrolyte at a potential scan rate of 50 mV/s for (a) a bare Au electrode, (b) the SAM of a 2-naphthalenethiol-modified Au electrode, and (c) an annealed electrode after the SAM formation.

We have also used hexaammineruthenium(III) chloride as a redox probe to determine the barrier property of the monolayer. Figure 5a−c shows the CVs obtained for the bare gold surface, SAM coated, and annealed electrodes, respectively. It can be seen from the figure that the ruthenium redox reaction is not blocked, even in the case of the annealed SAM electrode, which is very much in contrast to the behavior of the potassium ferrocyanide redox system. It can be seen that the monolayer-coated electrode shows nearly reversible peaks for the ruthenium redox reaction, showing the facile nature of the electron-transfer process with the reaction under diffusion control.

Figure 6 shows the impedance plots for the bare gold and SAM-modified electrodes (including the potential-cycled and annealed electrodes) in 1 mM hexaammineruthenium(III) chloride with 0.1 M $LiClO_4$ as the supporting electrolyte at the formal potential. The equivalent circuit-fitting analysis of the impedance plots shows that there is a small increase in the R_{ct} values for the SAM-modified electrodes when compared with the bare gold electrodes. The high-frequency part of the impedance data shows a small semicircle, as can be seen from the inset of the respective diagrams. The impedance analysis also indicates that there is a small increase in R_{ct} value with the potential-cycling and annealing processes. This implies that the electron-transfer process is not significantly inhibited in the case of the ruthenium redox reaction. Because the electron-transfer reaction is almost fully inhibited in the case of ferrocyanide ions, which have a comparable ionic size (0.64 nm for the ruthenium hexaammine complex vs 0.60 nm for the potassium ferrocyanide complex),[8e] it is difficult to conclude that ruthenium ions can have access to the electrode surface through the pinholes and defects present in the monolayer and ferrocyanide ions cannot.

The electron-transfer reaction on the SAM-modified gold electrodes can occur either through pinholes and defects present in the monolayer or by a tunneling process. In the case of aromatic thiols, the electron transfer can be further facilitated by the delocalized π-electrons present in the molecule because

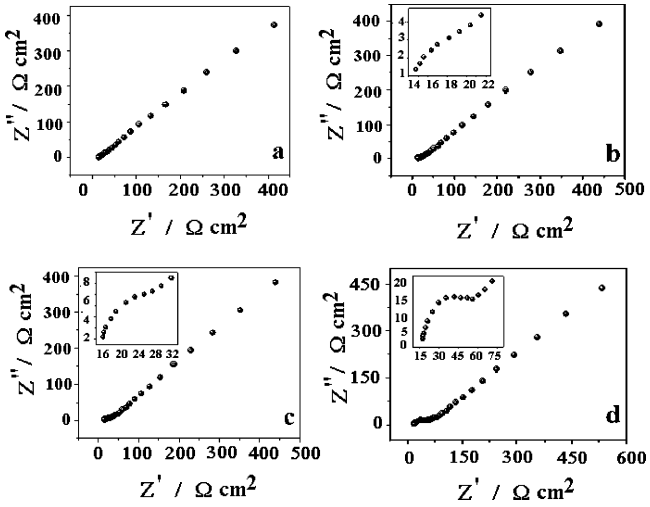

Figure 6. Impedance plots in 1 mM hexaammineruthenium(III) chloride with 0.1 M $LiClO_4$ as supporting electrolyte for (a) a bare Au electrode, (b) the SAM of a 2-naphthalenethiol-coated Au electrode, (c) a potential-cycled electrode after the monolayer formation, and (d) an annealed electrode after the monolayer formation. Insets show the zoomed impedance plots of the above-mentioned electrodes at a high-frequency region, indicating the marginal increase in R_{ct} values of the respective electrodes.

of extended conjugation. It is well-known that the long-chain aliphatic thiols form a well-packed, highly dense monolayer free of measurable pinholes and act as a barrier to electron-transfer reactions and ion penetration. If the electron transfer occurs through the pinholes and defects present in the monolayer, then the response of the cyclic voltammogram will depend on the distribution of pinholes and defects present in the structure of the monolayer. A linear diffusion process is expected when the pinholes are close enough for the diffusion layers to be overlapping with each other, facilitating the electron-transfer reaction. If the pinholes and defects are more widely spaced and evenly distributed, then there is no overlap of the diffusion layer and the pores constitute an array of microelectrodes, leading to radial diffusion. In the case of SAMs of 2-naphthalenethiol on Au, the response obtained in the cyclic voltammogram of $[Fe(CN)_6]^{3-|4-}$ (Figure 1b) shows that the linear diffusion is dominant and the electron transfer occurs through the gaps available in the monolayer. The potential-cycling effect leads to an effective packing of the monolayer with much fewer pinholes and defects (Figure 3b). After annealing, the radial diffusion process dominates and the electrode behaves like a microelectrode array with excellent blocking of the redox reaction (Figure 3c).

We have carried out several experiments intended to evaluate the integrity of the monolayer and to rule out the possibility of any reaction product blocking the $[Fe(CN)_6]^{3-|4-}$ redox reaction. One of the experiments involved first carrying out CV studies in the potential range from -0.4 to $+0.1$ V vs SCE, corresponding to that of the $[Ru(NH_3)_6]^{2+|3+}$ redox reaction where a reversible CV is obtained. This is followed by scanning the same electrode in the potential region from -0.1 to $+0.5$ V vs SCE, corresponding to the $[Fe(CN)_6]^{3-|4-}$ redox reaction. Here, the CV shows a fully blocking behavior. Further scanning at the potential range of the $[Ru(NH_3)_6]^{2+|3+}$ redox reaction again exhibits a reversible CV. From these experiments, we show that the monolayer is neither desorbed nor undergoes any structural transformation within these potential ranges (see Supporting Information I). These studies also prove that 2-naphthalenethiol does not undergo any redox reaction within the potential range of our study.

We have also studied the potential dependence of interfacial capacitance (see Supporting Information II). These studies clearly indicate that the monolayer is stable and intact on the electrode surface at the potential range used for the study of the electron-transfer processes of both ferrocyanide and hexaammineruthenium redox reactions. The measured capacitance values in 1 M NaF also do not show any large changes within the potential range -0.6 to $+0.8$ V vs SCE, except at extreme ranges used for the analysis. This means that the 2-naphthalenethiol does not desorb or undergo any redox reaction on the electrode surface at this potential range. It is also clear from these studies that a potential-dependent structural change of the monolayer has not occurred at the potential range of the $[Ru(NH_3)_6]^{2+|3+}$ redox reaction, which would have been reflected in an abnormal increase in the capacitance value. This also rules out the possibility of the hexaammineruthenium(III) species penetrating through the film and undergoing a redox reaction.

The fact that the annealed monolayer completely blocks the electron-transfer reaction in the case of the ferrocyanide system and allows the ruthenium redox reaction shows that the SAM, far from acting as an effective barrier, actually facilitates the electron-transfer reaction of the ruthenium complex. It is well-known that the hexaammineruthenium(III) chloride undergoes an outer-sphere electron-transfer reaction in which the redox species approaches the SAM-modified electrode surface and exchanges electrons with the metal at a minimal distance, with the hydration shell remaining intact.[19] This is in contrast to that of the redox reaction of the potassium ferro/ferricyanide system, which involves the formation of reaction intermediates that get adsorbed on the electrode surface. In this case, the electron transfer is accompanied by a change in the structure of the coordination shell, thereby involving bond rearrangements.[20] We feel that such a process is inhibited because of inaccessibility of the electrode surface to the redox species. The electron-transfer process in the case of the hexaammineruthenium(III) chloride reaction can take place by tunneling, provided that the process is facilitated by a suitable mediator. The tunneling process via the alkyl chain is well-known in the case of alkanethiols[21] and oligophenylenevinylene bridges between a gold electrode and a tethered redox species in contact with an aqueous electrolyte.[22] However, the electron transfer by tunneling will exhibit distance dependence, and when the redox species is separated by several angstroms from the surface, the process should slow and follow charge-transfer kinetics. For a distant-dependent electron transfer for a donor−bridge−acceptor system, the current (I) is exponentially related to the distance separating the centers of the donor−acceptors (R) by the relationship $I \propto e^{-\beta R}$, where β is the inverse decay length, a structure-related attenuation factor for the SAM. Although this factor is around 0.8 $Å^{-1}$ for alkanethiols,[21d] it is generally low (0.1−0.6 $Å^{-1}$) for oligophenylenethiols[23] and other conjugated oligomers,[24] which is attributed to delocalization of donor and acceptor states on the bridge.

The fact that the reaction is not inhibited to a significant extent and is under diffusion control at lower frequencies points to a tunneling process where the π-electrons in the naphthalene ring facilitate the electron transfer between the ruthenium complex and the gold electrode. It has been previously reported that, in the case of both aromatic and heteroaromatic thiols, the electron-transfer reaction is facilitated by the presence of highly delocalized π-electrons in the aromatic ring and also by the extended conjugation of the molecules.[25−27] This property of

the aromatic SAM is extensively used for sensor and catalysis applications.[28−30] The aromatic SAM can also be used as a molecular bridge to study the effects of different interaction forces and ionic and hydrogen bonding in the long-range electron-transfer reaction. The observed results were attributed to the tunneling process because of the presence of delocalized π-electrons in the aromatic ring, which acts as a bridge between the electrode surface and the redox probe.[31−33] In our case, the facile nature of the electron-transfer reaction of the ruthenium complex at the SAM−solution interface suggests a tunneling process, where the naphthalene ring with the delocalized π-electrons acts as a bridge between the monolayer-modified electrode and the ruthenium complex.

3.3. Study of Kinetics of Adsorption of 2-Naphthalenethiol on Au. Although the kinetics of adsorption of alkanethiol SAMs on gold has been well studied,[34] there are very few reports in the literature on the kinetics of SAM formation of aromatic thiols. A study of the adsorption kinetics provides information on the monolayer evolution and structural organization with time. In the case of alkanethiol, the kinetics of monolayer formation is fairly clear. The adsorption process generally follows the Langmuir kinetics at higher concentrations and the diffusion-controlled Langmuir model at lower concentrations of aliphatic thiols.[34]

In the present work, we have studied the adsorption kinetics of 2-naphthalenethiol on gold using electrochemical impedance spectroscopy. In electrochemical systems, one of the earliest methods used for the study of adsorption kinetics was the measurement of interfacial capacitance.[35] It is well-known that the capacitance of the electrical double layer precisely describes the adsorption properties and is being used widely in the study of self-assembled monolayers.[36] The monolayer forms a dielectric barrier between the metal and the electrolyte. The interfacial capacitance of a metal−SAM−electrolyte interface consists of a series combination of the capacitance of the SAM and the capacitance of the diffuse layer. The overall capacitance is dominated by the smaller of the two, namely, the capacitance of the SAM.[1]

The adsorption kinetics of the 2-naphthalenethiol monolayer on Au has been followed by measuring the impedance as a function of time using a 10 μM solution of 2-naphthalenethiol and 0.1 M $LiClO_4$ in ethanol. The SAM formation kinetics was carried out at two different potentials, viz., 0 and 0.175 V vs SCE. From the imaginary component of impedance at the high-frequency pseudoplateau region, the capacitance of the monolayer was measured as a function of time.[34d,e] The surface coverage (θ) was obtained using the formula

$$\theta = (C_0 - C_i)/(C_0 - C_f) \quad (1)$$

where C_0 is the bare gold capacitance, C_i is the capacitance at any time t, and C_f is the capacitance of the fully covered monolayer. Figure 7a,b shows the plots of surface coverage with time for two different potential values. There are two distinct time constants that can be seen from the θ vs t plots. During the first, fast step (from 0 to ca. 150 s), almost 80−85% of coverage is completed, and the second, slower step (150−1000 s) extends to almost complete coverage of the monolayer. We have fitted the data up to 1000 s. However, it can be seen from the figures that the complete coverage occurs beyond 3000 s. We have observed some fluctuations in the surface coverage values beyond 2000 s, as can be seen from Figure 7. However, such a behavior had not been reported in the case of adsorption of alkanethiols on Au.[34] These fluctuations signify the rearrangement of molecules on the surface during the monolayer formation. We have calculated rate constants for the adsorption kinetics on the basis of Langmuir and diffusion-controlled Langmuir (DCL) adsorption isotherms, which are represented as

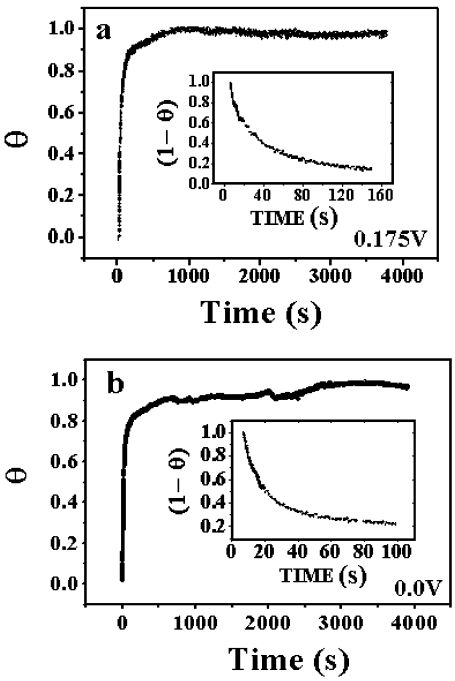

Figure 7. Surface coverage (θ) vs time plots for 10 μM 2-naphthalenethiol and 0.1 M $LiClO_4$ in ethanol at potentials (a) 0.175 V and (b) 0 V vs SCE. The insets show the plots of $(1 - \theta)$ vs time during the initial duration of the adsorption, corresponding to the first time constant.

$$\theta(t) = [1 - \exp(-k_m t)] \quad (2)$$

$$\theta(t) = [1 - \exp(-k_m \sqrt{t})] \quad (3)$$

where $\theta(t)$ is the surface coverage at any instant time t and k_m is the rate constant of adsorption.

The insets of Figure 7a,b show the plots of $(1 - \theta)$ vs time for the duration of the first time constant for the respective potentials. We obtained an excellent fit for these plots using Langmuir adsorption isotherms. We found that the rate constant values obtained from the first time constant, k_m, for 2-naphthalenethiol adsorption varies with the applied potential, viz., 0.0588 and 0.0379 s^{-1} for 0 and 0.175 V vs SCE, respectively. The initial rate of adsorption is distinctly faster at 0 V vs SCE. However, the full coverage is reached only beyond 2500 s. In the case of 0.175 V vs SCE, though the initial rate of adsorption is slower, the full coverage is reached at the end of 1000 s. We have used the concentration independent rate constant k_a as a comparison with the rate of adsorption of alkanethiols, as reported in the literature.[34] We find that the k_a value obtained for 2-naphthalenethiol at 0.175 V vs SCE is comparable to that of the alkanethiol value of about 2800 M^{-1} s^{-1}.[34d] However, the rate of adsorption, k_a, of 5880 M^{-1} s^{-1} at 0 V vs SCE is much higher.

The interfacial capacitance value of the SAM-modified electrode was determined to be 2.76 ± 0.13 μF cm^{-2}, which is somewhat higher than the theoretical value of the capacitance for the SAM of 2-naphthalenethiol on Au obtained using the expression

$$C = \epsilon\epsilon_0 A/d \quad (4)$$

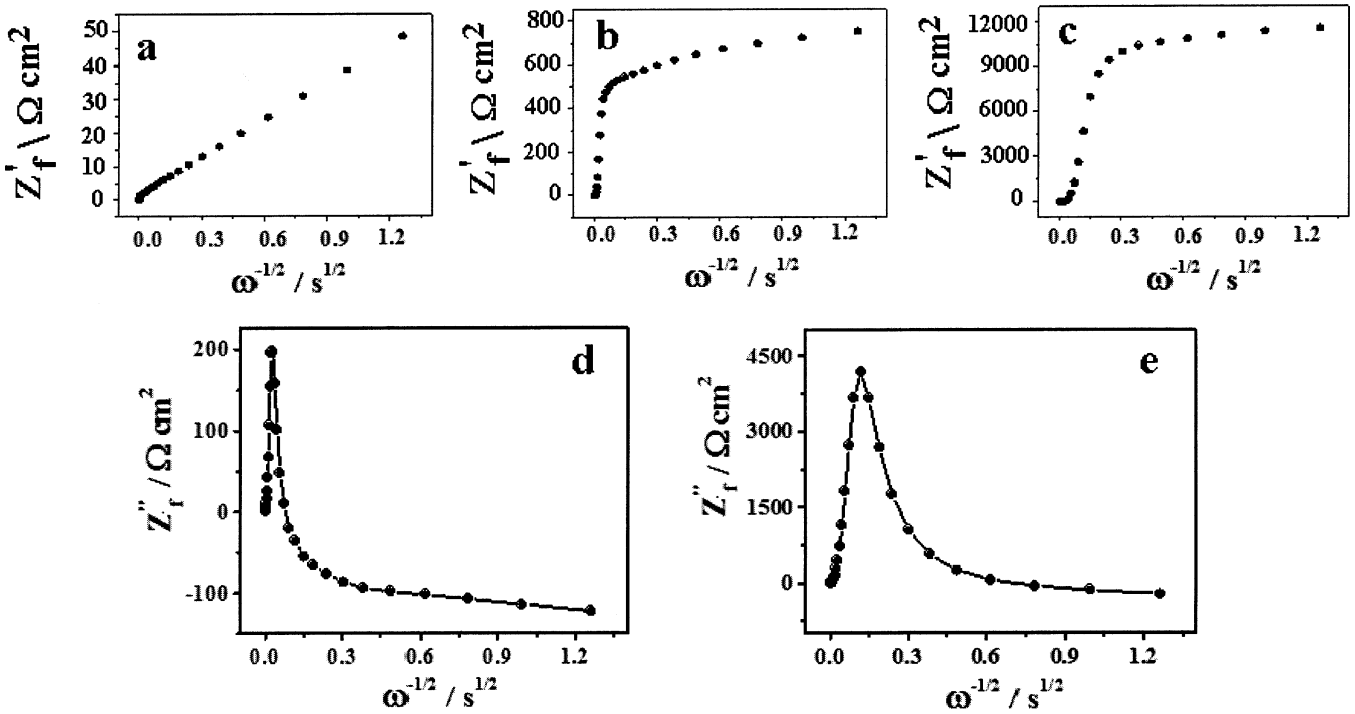

Figure 8. Plots of real parts of the faradaic impedance Z'_f vs $\omega^{-1/2}$ for (a) a bare Au electrode, (b) the SAM of a 2-naphthalenethiol-coated Au electrode, (c) an annealed electrode after the SAM formation, (d) plots of imaginary parts of the faradaic impedance (Z''_f) as a function of $\omega^{-1/2}$ for the SAM of a 2-naphthalenethiol-modified Au electrode, and (e) an annealed electrode after the monolayer formation.

where C is the capacitance, ϵ is the dielectric constant, ϵ_0 is the permittivity of vacuum, and d is the thickness of the monolayer. From the measured capacitance value, using the above equation, we have calculated the thickness of the monolayer to be 8.02 Å. Because the molecular length of 2-naphthalenethiol is 9.3 Å, the lower value of the monolayer thickness obtained implies that the molecules are tilted from the surface normal. From the molecular length of 9.3 Å for 2-naphthalenethiol and a monolayer thickness of 8.02 Å, we have determined the tilt of the molecule to be about 30° from the Au surface normal.

3.4. Pore Size Analysis of the 2-Naphthalenethiol SAM. Electrochemical impedance spectroscopic studies can provide valuable information on the pinholes and defects in the monolayer. Finklea et al.[37] developed a model for the impedance response of a monolayer-modified electrode, which behaves as an array of microelectrodes. Fawcett and co-workers have extensively studied the monolayer integrity by pore size analysis using electrochemical impedance data.[38] On the basis of the work of Matsuda[39] and Amatore,[40] a model has been developed to fit the faradaic impedance data obtained for the electron-transfer reactions at the SAM-modified electrode to understand the distribution of pinholes in the monolayer. The impedance expressions have been derived by assuming that the total pinhole area fraction, $(1 - \theta)$, is less than 0.1, where θ is the surface coverage of the monolayer. Both the real and imaginary parts of the faradaic impedance values are plotted as a function of $\omega^{-1/2}$. There are two limiting cases for this theory to be applied. At higher frequencies, the diffusion profiles of each individual microelectrode constituent of the array are separated, in contrast to the situation at lower frequencies where there is an overlap.

In the case of the SAM of 2-naphthalenethiol on Au, the presence of pinholes and defects is analyzed using the above-mentioned model. Figure 8a−e shows the real and imaginary parts of the faradaic impedance of different systems plotted as a function of $\omega^{-1/2}$. For comparison, the plot of a bare gold electrode is also shown (Figure 8a). Figure 8b,c shows the plots of real components of faradaic impedance, Z'_f vs $\omega^{-1/2}$, for the monolayer-coated electrode and annealed SAM electrodes, respectively. Figure 8d,e shows the plots of imaginary components of the faradaic impedance, Z''_f vs $\omega^{-1/2}$, for the respective electrodes. The faradaic impedance plots show the features similar to those of an array of microelectrodes. There are two linear domains at high and low frequencies for the Z'_f vs $\omega^{-1/2}$ plot and a peak formation in the Z''_f vs $\omega^{-1/2}$ plot corresponding to the frequency of transition between the two linear domains. According to the model proposed, this frequency separates the two time-dependent diffusion profiles for the microelectrodes.

The surface coverage of the monolayer can be obtained from the slope of the Z'_f vs $\omega^{-1/2}$ plot at a higher frequency region and is given by

$$m = \sigma + \sigma/(1 - \theta) \tag{5}$$

where m is the slope, θ is the surface coverage of the monolayer, and σ is the Warburg coefficient, which can be obtained from the unmodified bare gold electrode.

From the analysis of Figure 8b,c, a surface coverage value of 99% is obtained for the monolayer-modified electrode, which increases to a value of 99.5% after the annealing effect. It is proposed that the thermal annealing process eliminates any trapped solvent molecules (ethanol) during the adsorption process and helps in the formation of a highly dense, well-packed, and compact monolayer.

3.5. Gold Oxide Stripping Analysis. The cyclic voltammogram of the gold electrode in 0.1 M $HClO_4$ shows the usual features due to gold oxide formation during the positive potential scanning and oxide stripping upon reversal of the scan direction. The quantity of electric charges passed during its removal of oxide is proportional to the effective-electrode area. By comparing the charge of a SAM-modified electrode with the respective charge of the bare gold electrode, we can measure the surface coverage of the monolayer qualitatively.

Figure 9 shows the cyclic voltammograms of gold oxidation in 0.1 M $HClO_4$. Figure 9a shows the gold oxide formation

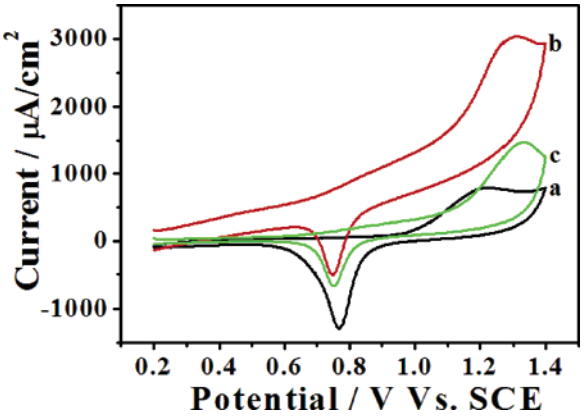

Figure 9. Cyclic voltammograms of gold oxide stripping analyses in 0.1 M $HClO_4$ for (a) a bare Au electrode, (b) the SAM of a 2-naphthalenethiol-modified Au electrode, and (c) an annealed SAM after the monolayer formation.

and the stripping peaks for a bare gold electrode. Figure 9b,c shows the CVs for the SAM of 2-naphthalenethiol on Au before and after thermal annealing, respectively. Compared with bare gold electrodes, the measured charge on the monolayer-modified electrodes is significantly less, as expected. It can be seen that the charge values measured for these two electrodes before and after annealing, from the cathodic stripping peaks, are almost the same (350 nC cm^{-2}). The area fraction of the coverage is calculated to be 0.95 from the formula $(1 - Q_{SAM}/Q_{Au})$, where Q_{SAM} and Q_{Au} are the charges measured for the monolayer-covered electrode and the bare gold electrode, respectively. This coverage fraction is much smaller than the value obtained from the impedance plot, viz., 0.99−0.995. This difference in the values can be attributed to the fact that smaller OH^- ions have easier access to the electrode compared with that of bulkier ferrocyanide ions, which are used as coverage probes in these two methods.

However, after 3−4 cycles in 0.1 M $HClO_4$, the voltammogram is almost similar to that of the bare gold electrode, indicating the complete removal of the monolayer. The desorption of the monolayer is confirmed by the fact that the potassium ferrocyanide electron-transfer reaction produces reversible peaks on the electrode which was subjected to the oxide stripping experiment. This indicates that the monolayer is not electrochemically stable when cycled to very high positive potentials.

3.6. Grazing-Angle FTIR Spectroscopy. We have carried out grazing-angle FTIR spectroscopy on the SAM of 2-naphthalenethiol on Au to characterize its orientation. Figure 10a,b shows the FTIR spectrum of the monolayer-modified Au surface before and after the annealing effect, respectively. The bulk spectrum of 2-naphthalenethiol is also shown in Figure 10c. The multiple peaks between 1600 and 1700 cm^{-1} are due to the aromatic ring C−C stretching mode. The peaks at 916 and 853 cm^{-1} are due to the out-of-plane bending modes of the aromatic C−H group. The presence of peaks due to the aromatic ring C−C stretching mode and out-of-plane bending of the aromatic C−H group imply that the naphthalene ring is not lying parallel to the Au surface. However, we do not see any peak at 3050 cm^{-1} due to the stretching mode of the aromatic ring C−H group, as it is obscured by the rapid fall of detector sensitivity in that region.

The striking feature of the two spectra is the positive shift in the wavenumber for the aromatic ring C−C stretching mode after annealing. There is a positive peak shift by ∼4−5 cm^{-1} which can be attributed to the formation of a highly ordered and compact monolayer after the annealing process. The

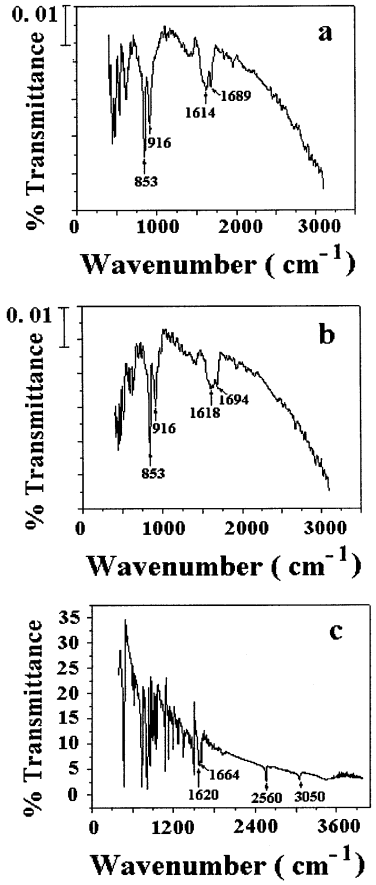

Figure 10. Grazing-angle FTIR spectra of (a) the monolayer of a 2-naphthalenethiol-coated Au electrode, (b) an annealed electrode after the monolayer formation, and (c) bulk 2-naphthalenethiol in KBr.

annealing effect improves the packing density of the monolayer by causing the aromatic ring moiety to be tilted slightly, thereby increasing the van der Waals interaction among the aromatic rings. These results show that the effect of annealing leads to the formation of a well-packed, highly oriented monolayer of 2-naphthalenethiol on Au.

3.7. Scanning Tunneling Microscopy (STM). STM studies have been used to characterize the structure of the monolayer at the molecular level and also to understand the nature of the adsorbed film. Figure 11a shows the constant current STM image of the bare gold surface, which was used to form the monolayer film at a 6 × 6 nm range. Though the atomic features could not be resolved, the surface has a predominantly Au(111) orientation, as determined by X-ray diffraction studies. Figure 11b shows the Fourier filtered constant height images of the 2-naphthalenethiol monolayer adsorbed on the evaporated gold surface at a 6 × 6 nm range. The chemisorbed S−S bond distance is determined to be 5 Å in the adjacent columns of the image (Figure 11c). The vertical bright spots correspond to the individual molecules of 2-naphthalenethiol adsorbed on Au. These molecules, which are arranged in diagonal rows, are separated by a distance of 8.4 Å. It can be seen that the area per molecule corresponds to 42 $Å^2$ (8.4 × 5 Å). This value almost exactly corresponds to the observed value of 41.4 $Å^2$ per naphthalene molecule on a smooth polycrystalline Au surface.[13] Again, from the STM image (Figure 11), the monolayer coverage on the gold surface is calculated to be about 4 × 10^{-10} mol per true surface area in cm^2 (the roughness factor of the gold surface used for STM measurements is 1.6). A closer look at the image shows that the high electron-density region

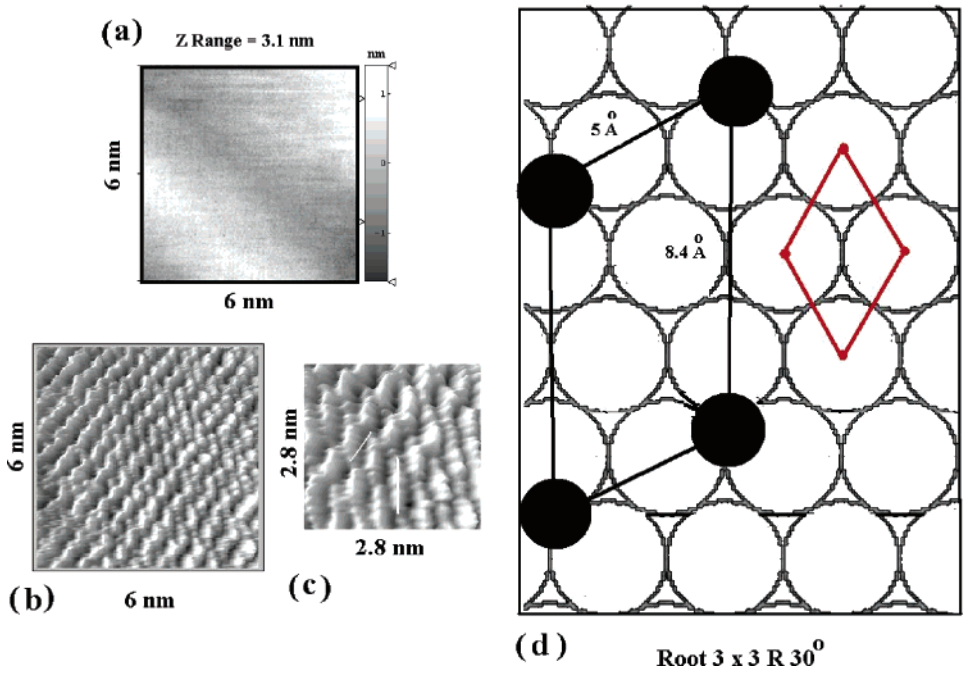

Figure 11. (a) STM image of a bare Au surface at a 6 × 6 nm range. (b) Constant height STM image of 2-naphthalenethiol adsorbed on the Au surface at a 6 × 6 nm scan range showing individual molecules. (c) Zoomed image of 2.8 × 2.8 nm. The slanted white line of 5 Å corresponds to the distance between sulfur atoms of adjacent columns of 2-naphthalenethiol molecules and the vertical line of 8.4 Å corresponds to the distance between the two sulfur atoms of adjacent rows of 2-naphthalenethiol molecules. (d) Model of adsorption of 2-naphthalenethiol on the Au surface and its structural orientation of a $\sqrt{3} \times 3$ R30° overlayer. The arrangement of the Au substrate atoms is shown by the diamond shape on the right.

in the individual molecular space spreads to about 6 Å, a rather large value for the naphthalene ring in upright orientation. This means that the molecule is canted with respect to the Au surface normal, which is in agreement with the earlier results of Kolega and Schlenoff.[13] This structural orientation of the naphthalene ring on a Au surface, obtained for the monolayer using STM, is again in conformity with our earlier results of both the electron-transfer reaction of the ruthenium complex (based on CV and EIS) and grazing-angle FTIR spectroscopy. The possible structure of 2-naphthalenethiol orientations on gold is modeled on the basis of the features of the molecular arrangement shown in Figure 11c. The schematic structure, with respect to the underlying gold surface, is shown in Figure 11d along with the dimensions. It can be seen that the surface structure can be described as a $\sqrt{3} \times 3$ R30° overlayer structure of 2-naphthalenethiol on gold.

4. Conclusions

We report in this work a self-assembled monolayer of 2-naphthalenethiol on Au, which has been characterized by electrochemical techniques, FTIR, and STM. The annealing of the SAM after formation produces a well-packed and compact monolayer, as shown by CV and EIS studies. The electron-transfer reaction of potassium ferrocyanide has been studied on the thiol-modified surface, which is found to occur mainly through the pinholes, defects, and domain boundaries in the film. In contrast, in the case of the ruthenium complex, the reaction is not significantly blocked. The electron-transfer process in this case is attributed to tunneling mediated by a π-electron bridge. The pinhole analysis, using electrochemical impedance data, shows a surface coverage of the 2-naphthalenethiol SAM to the extent of >99%. The STM studies of 2-naphthalenethiol molecules show that their rings are tilted to the surface normal with the formation of a $\sqrt{3} \times 3$ R30° overlayer structure.

Acknowledgment. We would like to thank Mr. M. Jayadeviah for help with STM imaging, Ms. K. N. Vasudha for help with FTIR, Mr. Ram for his skillful work in preparing the evaporated gold samples, and Mr. A. Dhason for fabricating the gold wire electrodes.

Supporting Information Available: Series of experiments to prove the selectivity of monolayers to the electron-transfer reaction of the ruthenium complex were discussed, and the cyclic voltammograms are shown in Figure S1. Measurement of potential dependence of interfacial capacitance on SAM-modified electrodes was carried out in 1 M NaF, and the results are shown in Figure S2. This material is available free of charge via the Internet at http://pubs.acs.org.

References and Notes

(1) (a) Finklea, H. O. Self-assembled Monolayers on Electrodes. In *Encyclopedia of Analytical Chemistry*; Meyers, R. A., Ed.; John Wiley & Sons Ltd: Chichester, U.K. (b) Ulman, A. *An Introduction to Ultrathin organic films from Langmuir-Blodgett to self-assembly;* Academic Press: San Diego, CA, 1991.

(2) (a) Hickman, J. J.; Ofer, D.; Laibinis, P. E.; Whitesides, G. M. *Science* **1991**, *252*, 688. (b) Mirkin, C. A.; Ratner, M. A. *Annu. Rev. Phys. Chem.* **1992**, *43*, 719. (c) Zhong, C. J.; Porter, M. D. *Anal. Chem.* **1995**, *67*, 709A. (d) Cornell, B. A.; Braach-Maksvytis, V. L. B.; King, L. G.; Osman, P. D. J.; Raguse, B.; Wieczorek, L.; Pace, R. J. *Nature* **1997**, *387*, 580.

(3) (a) Tariov, M. J.; Burgess, D. R. F.; Gillen, G. *J. Am. Chem. Soc.* **1993**, *115*, 5305. (b) Huang, J.; Dahlgren, D. A.; Hemminger, J. C. *Langmuir* **1994**, *10*, 626. (c) Wollman, E. W.; Kang, D.; Frisbie, C. D.; Larcovic, T. M.; Wrighton, M. S. *J. Am. Chem. Soc.* **1994**, *116*, 4395.

(4) Li, D.; Ratner, M. A.; Marks, T. J.; Znang, C. H.; Yang, J.; Wong, G. K. *J. Am. Chem. Soc.* **1990**, *112*, 7389.

(5) Kawanishi, Y.; Tamaki, T.; Sakuragi, M.; Seki, T.; Swuzki, Y.; Ichimura, K. *Langmuir* **1992**, *8*, 2601.

(6) (a) Laibinis, P. E.; Whitesides, G. M. *J. Am. Chem. Soc.* **1992**, *114*, 9022. (b) Ohno, N.; Uehara, J.; Aramaki, K. *J. Electrochem. Soc.* **1993**, *140*, 2512.

(7) Ulman, A. *Chem. Rev.* **1996**, *96*, 1533.

(8) (a) Sabatani, E.; Cohen-Boulakia, J.; Bruening, M.; Rubinstein, I. *Langmuir* **1993**, *9*, 2974. (b) Frey, S.; Stadler, V.; Heister, K.; Eck, W.; Zharnikov, M.; Grunze, M. *Langmuir* **2001**, *17*, 2408. (c) Hayes, A. W.; Shannon, C. *Langmuir* **1996**, *12*, 3688. (d) Batz, V.; Schneeweiss, M. A.; Kramer, D.; Hagenstrom, H.; Kolb, D. M.; Mandler, D. *J. Electroanal. Chem.* **2000**, *491*, 55. (e) Chailapakul, O.; Crooks, R. M. *Langmuir* **1995**, *11*, 1329.

(9) (a) Aslam, M.; Bandyopadhyay, K.; Vijayamohanan, K.; Lakshminarayanan, V. *J. Colloid Interface Sci.* **2001**, *234*, 410. (b) Bandyopadhyay, K.; Vijayamohanan, K. *Langmuir* **1998**, *14*, 625. (c) Bandyopadhyay, K.; Vijayamohanan, K.; Venkataramanan, M.; Pradeep, T. *Langmuir* **1999**, *15*, 5314. (d) Venkataramanan, M.; Skanth, G.; Bandyopadhyay, K.; Vijayamohanan, K.; Pradeep, T. *J. Colloid Interface Sci.* **1999**, *212*, 553. (e) Bandyopadhyay, K.; Sastry, M.; Paul, V.; Vijayamohanan, K. *Langmuir* **1997**, *13*, 866. (f) Bandyopadhyay, K.; Vijayamohanan, K.; Shekhawat, G. S.; Gupta, R. P. *J. Electroanal. Chem.* **1998**, *447*, 11.

(10) Wooster, T. T.; Gamm, P. R.; Geiger, W. E. *Langmuir* **1996**, *12*, 6616.

(11) Chang, S.; Chao, I.; Tao, Y. *J. Am. Chem. Soc.* **1994**, *116*, 6792.

(12) Hagg, R.; Rampi, M. A.; Holmlin, R. E.; Whitesides, G. M. *J. Am. Chem. Soc.* **1999**, *121*, 7895.

(13) Kolega, R. R.; Schlenoff, B. J. *Langmuir* **1998**, *14*, 5469.

(14) Jayadevaiah, M.; Lakshminarayanan, V. *Meas. Sci. Technol.* **2004**, *15*, N35.

(15) Bruce Lennox, R.; Boubour, E. *J. Phys. Chem. B* **2000**, *104*, 9004.

(16) Bruce Lennox, R.; Boubour, E. *Langmuir* **2000**, *16*, 7464.

(17) Anderson, M. R.; Gatin, M. *Langmuir* **1994**, *10*, 1638.

(18) Paik, W.; Eu, S.; Lee, K.; Chon, S.; Kim, M. *Langmuir* **2000**, *16*, 10198.

(19) Blumberger, J.; Sprik, M. *J. Phys. Chem. B* **2005**, *109*, 6793.

(20) Fleischmann, M.; Graves, P. R.; Robinson, J. *J. Electroanal. Chem.* **1985**, *182*, 87.

(21) (a) Chidsey, C. E. D. *Science* **1991**, *251*, 919. (b) Smalley, J. F.; Feldberg, S. W.; Chidsey, C. E. D.; Linford, M. R.; Newton, M. D.; Liu, Y. *J. Phys. Chem.* **1995**, *99*, 13141. (c) Weber, K.; Hockett, L.; Creager, S. *J. Phys. Chem. B* **1997**, *101*, 8286. (d) Wang, W.; Lee, T.; Reed, M. A. *J. Phys. Chem. B* **2004**, *108*, 18398.

(22) Sikes, H. D.; Smalley, J. F.; Dudek, S. P.; Cook, A. R.; Newton, M. D.; Chidsey, C. E. D.; Feldberg, S. W. *Science* **2001**, *291*, 1519.

(23) Davis, W. B.; Svec, W. A.; Ratner, M. A.; Wasieiewski, M. R. *Nature* **1998**, *396*, 60.

(24) Lewis, F. D.; Liu, J.; Weigel, W.; Rettig, W.; Kurnikov, I. V.; Beratan, D. N. *Proc. Natl. Acad. Sci. U.S.A.* **2002**, *99*, 12536.

(25) Krings, N.; Strehblow, H.-H.; Kohnert, J.; Martin, H.-D. *Electrochim. Acta* **2003**, *49*, 167.

(26) Rampi, M. A.; Whitesides, G. M. *Chem. Phys.* **2002**, *281*, 373.

(27) Jin, Q.; Rodriguez, J. A.; Li, C. Z.; Darici, Y.; Tao, N. J. *Surf. Sci.* **1999**, *425*, 101.

(28) Retna Raj, C.; Takeo Ohsaka *J. Electroanal. Chem.* **2003**, *540*, 69.

(29) Sawaguchi, T.; Mizutani, F.; Yoshimoto, S.; Taniguchi, I. *Electrochim. Acta* **2000**, *45*, 2861.

(30) Yang, Y.; Khoo, S. B. *Sens. Actuators, B* **2004**, *97*, 221.

(31) Yu, H. Z.; Xia, N.; Zhang, J.; Liu, Z. F. *J. Electroanal. Chem.* **1998**, *448*, 119.

(32) Guo, L. H.; Facci, J. S.; Mclendon, G. *J. Phys. Chem.* **1995**, *99*, 4106.

(33) Guo, L. H.; Facci, J. S.; Mclendon, G. *J. Phys. Chem.* **1995**, *99*, 8458.

(34) (a) Karpovich, D. S.; Blanchard, G. J. *Langmuir* **1994**, *10*, 3315. (b) Dannenberger, O.; Buck, M.; Grunze, M. *J. Phys. Chem. B* **1999**, *103*, 2202. (c) Ron, H.; Rubinstein, I. *J. Am. Chem. Soc.* **1998**, *120*, 13444. (d) Subramanian, R.; Lakshminarayanan, V. *Electrochim. Acta* **2000**, *45*, 4501. (e) Yan, D.; Saunders, J. A.; Jennings, G. K. *Langmuir* **2002**, *18*, 10202.

(35) Damaskin, B. B.; Petrii, O. A.; Batrakov, V. V. *Adsorption of Organic compounds on Electrodes*; Plenum Press: New York, 1971.

(36) Finklea, H. O. In *Electroanalytical Chemistry, A Series of Advances*; Bard, A. J., Rubinstein, I., Eds.; Marcel Dekker: New York, 1996; Vol. 19, p 166.

(37) Finklea, H. O.; Snider, D.; Fedyk, J.; Sabatani, E.; Gafni, Y.; Rubinstein, I. *Langmuir* **1993**, *9*, 3660.

(38) (a) Protsailo, L. V.; Fawcett, R. *Langmuir* **2002**, *18*, 8933. (b) Protsailo, L. V.; Fawcett, R.; Russell, D.; Meyer, L. R. *Langmuir* **2002**, *18*, 9342. (c) Janek, R. P.; Fawcett, R.; Ulman, A. *Langmuir* **1998**, *14*, 3011.

(39) Tokuda, K.; Gueshi, T.; Matsuda, H. *J. Electroanal. Chem.* **1979**, *102*, 41.

(40) Amatore, C.; Saveant, J. M.; Tessler, D. J. *J. Electroanal. Chem.* **1983**, *147*, 39.